Ground Motion in Anchorage, Alaska, from the 2002 Denali Fault Earthquake: Site Response and Displacement Pulses

by David M. Boore

Abstract Data from the 2002 Denali fault earthquake recorded at 26 sites in and near Anchorage, Alaska, show a number of systematic features important in studies of site response and in constructing long-period spectra for use in earthquake engineering. The data demonstrate that National Earthquake Hazards Reduction Program (NEHRP) site classes are a useful way of grouping stations according to site amplification. In general, the sites underlain by lower shear-wave velocities have higher amplification. The amplification on NEHRP class D sites exceeds a factor of 2 relative to an average of motions on class C sites. The amplifications are period dependent. They are in rough agreement with those from previous studies, but the new data show that the amplifications extend to at least 10 sec, periods longer than considered in previous studies. At periods longer than about 14 sec, all sites have motion of similar amplitude, and the ground displacements are similar in shape, polarization, and amplitude for all stations.

The displacement ground motion is dominated by a series of four pulses, which are associated with the three subevents identified in inversion studies (the first pulse is composed of P waves from the first subevent). Most of the high-frequency ground motion is associated with the S waves from subevent 1. The pulses from subevents 1 and 2, with moment releases corresponding to **M** 7.1 and 7.0, are similar to the pulse of displacement radiated by the **M** 7.1 Hector Mine earthquake. The signature from the largest subevent (**M** 7.6) is more subdued than those from the first two subevents. The two largest pulses produce response spectra with peaks at a period of about 15 sec. The spectral shape at long periods is in good agreement with the recent 2003 NEHRP code spectra but is in poor agreement with the shape obtained from Eurocode 8.

Introduction

Anchorage, Alaska, is built on the edge of a deep sedimentary basin at the foot of the Chugach Mountains. The maximum thickness of the Quaternary and early middle Tertiary basin sediments is more than 7 km at a point about 150 km southwest of Anchorage, and the basin thickness exceeds 1 km in the western part of the city (Hartman *et al.*, 1974). The Quaternary deposits under Anchorage include Pleistocene glacial deposits and the silt and clay of the Bootlegger Cove formation (Dutta *et al.*, 2001). Shear-wave velocities, measured at 36 sites in the basin (Nath *et al.*, 1997; Dutta *et al.*, 2000), show that most of the city is built on deposits that fall within National Earthquake Hazards Reduction Program (NEHRP) site classes C and D (Fig. 1) (NEHRP site classes are defined in terms of the time-averaged velocities of shear waves to 30 m, as follows: A, greater than 1500 m/sec; B, between 1500 and 760 m/sec; C, between 760 and 360 m/sec; D, between 360 and 180 m/sec; E, less than 180 m/sec). The combination of the low-velocity sediments and the metamorphic bedrock is ideal for the amplification of seismic waves, and a number of empirical site-amplification studies have been published for the Anchorage area. These studies include generalized inversion (Dutta *et al.*, 2001) and horizontal-to-vertical spectral ratios (Nath *et al.*, 2002) of weak-motion data from a temporary network of stations. A permanent network of strong- and weak-motion stations was installed after the success of the temporary network. Several studies of site response using weak- and strong-motion recordings from the new network have been published, including the use of spectral ratios (Martirosyan *et al.*, 2002) and generalized inversion (Dutta *et al.*, 2003). These last two studies computed site response at the basin stations relative to a reference site in the nearby Chugach Mountains. All of the studies focused on site response within the 0.5 to 11 Hz frequency range, and not surprisingly, all of the studies found significant frequency-dependent site amplifications on the sediments beneath the
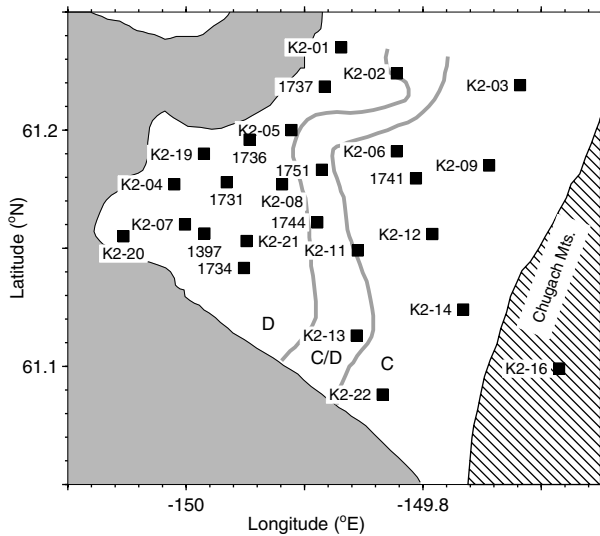
Figure 1. Location of stations and NEHRP site classes (site classes and base map from Fig. 12 by Martirosyan *et al.*, 2002). The C/D class is intermediate between NEHRP classes C and D and is defined by Martirosyan *et al.* (2002) by the average shear-wave velocity to 30 m being between 320 and 410 m/sec.

city. Although the detailed site-specific findings differ amongst the studies, they all find on average that the largest site amplifications are on the lower-velocity class D sites, with average amplifications around 3 at low frequencies (0.5–2.5 Hz) and around 1.5 at higher frequencies (3.0–7.0 Hz).

The 2002 **M** 7.9 Denali fault earthquake was well recorded on digital strong-motion instruments deployed in the Anchorage metropolitan area. These recordings provide an opportunity to compare site amplifications with those from the earlier studies, which used data from many events, and more importantly, are rich enough in low-frequency content that the site amplifications can be computed at lower frequencies than in the previous studies. I find that site amplification extends to periods of about 14 sec.

In addition to studies of site amplification, I discuss the individual pulses of ground displacement on the records. The displacement pulses are similar to those from the much smaller **M** 7.1 Hector Mine, California, earthquake. The pulses are of long-enough period to be relatively insensitive to local variations in site geology, and they produce a local increase in response spectra at periods between 10 and 20 sec. In addition, the pulses show site-independent but pulse-dependent polarizations. Interestingly, most of the high-frequency content in the ground motion is carried by the *S*-wave pulse produced by subevent 1. These observations are consistent with the results of Frankel (2004).

Data Processing and Characteristics

The data analyzed in this article were obtained on force-balance accelerometers whose response is flat to acceleration from 0 to 50 Hz. The sensor output was recorded on data-loggers with 114 db dynamic range at 200 samples per second. The data were provided by the U.S. Geological Survey (USGS) and the University of Alaska and are available from nsmp.wr.usgs.gov. The stations are plotted in Figure 1. Almost all data had drifts in displacement derived from double integration of the acceleration trace. To eliminate these drifts, the data were processed using simple baseline corrections and low-cut filtering with a second-order acausal 0.02 Hz butterworth filter; similar results were obtained using longer-period filters.

The three components of ground displacement at two sites underlain by very different materials are shown in Figure 2. The station K2-20 has a strong broadband site response centered at about 0.2 Hz, which leads to the increased chatter as compared to the recordings at K2-16 (see gray curves in Fig. 2). By filtering out high frequencies to eliminate this chatter, it is clear that the longer-period motions at these two dissimilar sites are comparable (see black curves in Fig. 2). The displacements are composed of four bursts of energy at times near 35, 70, 100, and 170 sec, labeled in Figure 2 as pulses 1, 2, 3, and 4, respectively. The waveforms do not have the dispersed character associated with waves traveling across thick sedimentary basins (e.g., Boore, 1999). Pulses 1 and 2 correspond to the *P*- and *S*-wave arrivals from what has been termed by Frankel (2004) as "subevent 1," interpreted as the thrust fault initiating the earthquake (the Susitna Glacier fault). Pulses 3 and 4 correspond to *S* waves from the strike-slip subevents 2 and 3 (Eberhart-Phillips *et al.*, 2003; Frankel, 2004). Subevent 2 was a concentrated zone of moment release on the portion of the Denali fault near the crossing of the Trans-Alaska Pipeline; subevent 3 occurred farther east. The moment releases on the three subevents corresponded to moment magnitudes 7.1, 7.0, and 7.6, respectively (Frankel, 2004).

Hodograms of the high-cut-filtered horizontal displacements at the two stations K2-20 and K2-16 are shown in Figures 3a and b for the four pulses identified in Figure 2. The polarizations are very similar for the same pulses on the two stations (and for the other stations, although not shown here), and the polarizations show a systematic clockwise rotation from pulse 2 through pulse 4. Frankel (2004) identifies pulses 1 and 2 as coming from subevent 1. The polarization for pulse 1 is consistent with *P* waves from that subevent, but pulse 2 is almost pure transverse motion, which at first seems inconsistent with radiation from an almost pure thrust fault (as found by Frankel, 2004). The *S*-wave radiation pattern for Frankel's fault orientation for the subevent 1-to-Anchorage azimuth (about 205°), however, is pure *SH* for takeoff angles of 15° and 105°. Because the actual waves composing the motion at Anchorage are probably made up of a series of arrivals corresponding to different takeoff angles, I am not sure if the values of the radiation pattern for a specific ray can be used to predict the polarization of the relatively long-period ground displacements. A more convincing argument for the consistency of the subevent 1
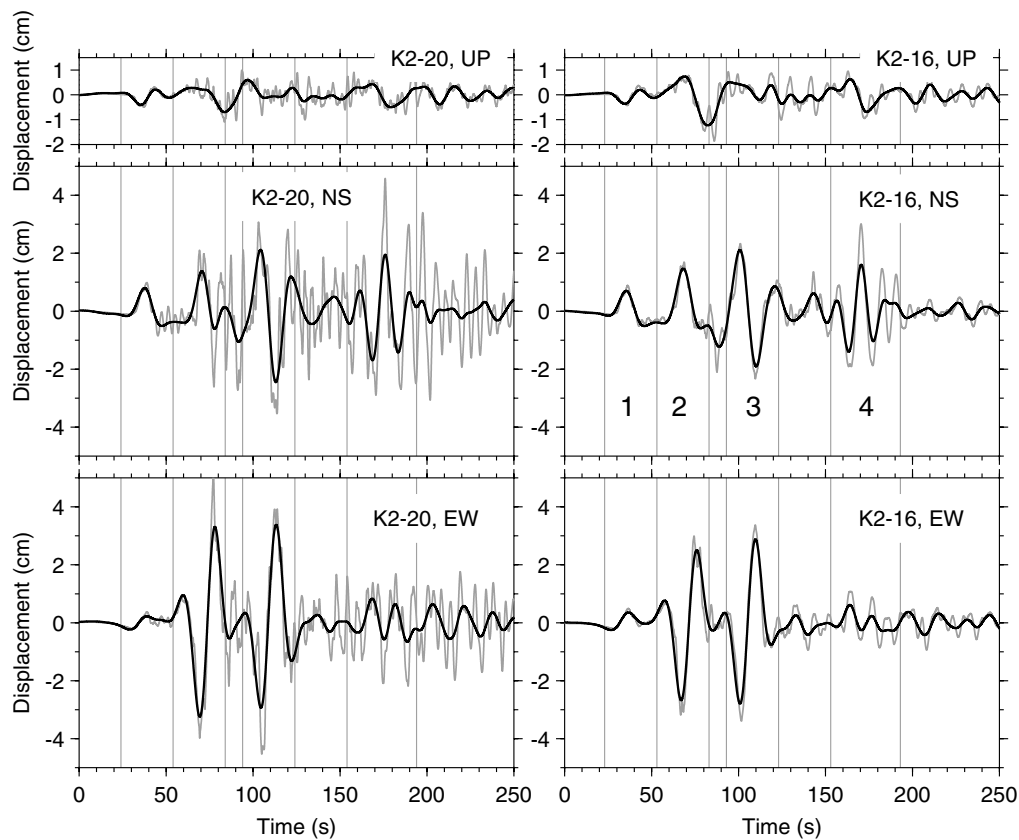
Figure 2. Displacements at stations K2-16 and K2-20, showing the strong (and differing) polarization of the four dominant displacement pulses. The vertical gray lines indicate the windows used in constructing hodograms (they are not at the same times for the two stations because the amount of pre-event motion was slightly different at the two stations; the record at K2-16 started 1 sec after that at K2-20, and I did not shift the records to align arrivals). Station K2-20 is on lower velocity materials and has more high frequency motion than does station K2-16. The numbers below the K2-16, NS trace label the pulses referred to in the text. Gray curves have been low-cut filtered at 0.02 Hz; black curves have been low-cut filtered at 0.02 Hz and high-cut filtered at 0.08 Hz.

mechanism and the observed polarization of pulse 2 is Frankel's waveform modeling, which produces a good fit to pulse 2 on both horizontal components in Anchorage, using the nearly-pure-thrust mechanism for subevent 1. The clockwise rotation of the polarization from pulse 3 to pulse 4 is consistent with *SH* waves being radiated from portions of the Denali fault at points progressively to the east and the southeast of the hypocenter (subevent 1). If composed of *SH* body and surface waves, pulse 4 seems to be coming from an azimuth of about 60° to 70° clockwise from north, which puts its source southeast of Frankel's subevent 3, possible along the Totschunda fault. Because his interpretations are based on careful study of a number of records obtained from various locations in Alaska, it is unlikely that subevent 3 has been mislocated by Frankel (2004). His waveform modeling underestimates the peak motions on the north–south component at Anchorage by about 20%, and thus the polarization for his model is counterclockwise relative to the observed polarization in Figure 3 and is consistent with *SH* polariza-

tion from subevent 3. This suggests that lateral refraction due to lateral changes in crustal structure may be producing small rotations in the observed polarization for certain travel paths.

Site Response

As indicated in the introduction, a number of previous studies have found significant and systematic site response in the Anchorage area, and therefore it will be no surprise to find the same for records of the Denali fault earthquake. The first indication of site response is in differences of peak acceleration, velocity, and displacements for the various stations. The corresponding time series are shown in Figure 4 for the same two stations used in the previous figures—K2-20 and K2-16 (the station in the Chugach Mountains). As noted before, these two stations are underlain by dissimilar near-surface materials. Note the increase of all three measures of ground shaking at K2-20 compared to K2-16, with
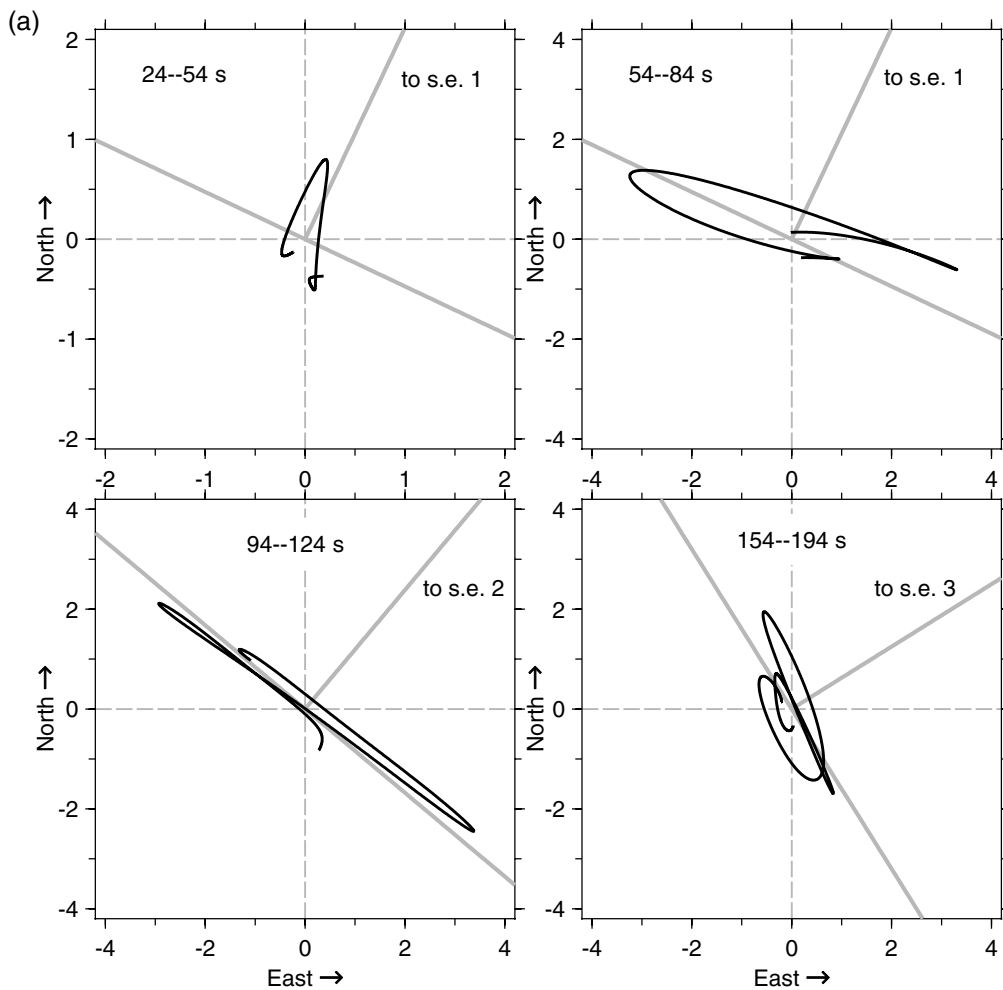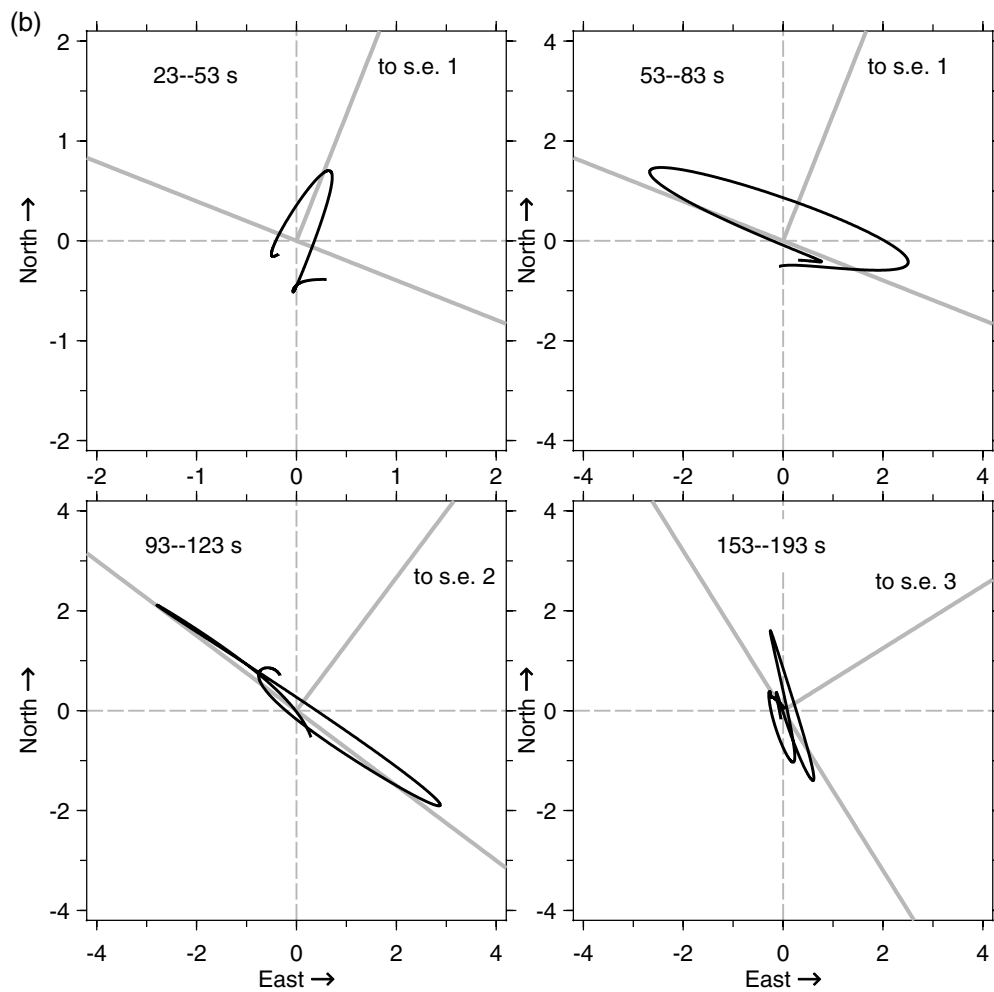
Figure 3. Hodograms of horizontal displacements in centimeters (bandpass filtered as in Figure 2) at (a) station K2-20 and (b) at station K2-16 for the four time windows indicated on Figure 2, showing the strong (and differing) polarization of the dominant displacement pulses. The azimuth from the station to the point of maximum moment release per km of faulting for each indicated subevent (s.e.) is shown, as well as the transverse direction to this azimuth. A 42.6° correction (U. Dutta, oral comm., 2003) has been applied to the orientation of the horizontal components. Note that the scale for the graph showing the displacements in the first time window is half that of the other graphs. (*continued*)

the greatest difference being for the higher-frequency motions. Also seen is something not obvious from plots of peak motions alone: the highest accelerations are associated with pulse 2, with little or no increase of accelerations at the arrival times of pulses 3 and 4 (I show later the influence of this difference on response spectra). This was noted by Frankel (2004) in his interpretation of envelopes of high-frequency ground motions.

Variation by NEHRP Site Class

Figure 5 shows plots of ratios of peak acceleration, peak velocity, and peak displacement relative to the average of motions recorded at class C sites. The amplifications for individual stations on different site classes are indicated by the

symbol used in the plot. An average of class C motions was used as the reference rather than the motions at station K2-16, on bedrock in the Chugach Mountains, because the K2-16 site seems to have its own amplification at frequencies above 7 to 8 Hz (Martirosyan and Biswas, 2002; Martirosyan *et al.*, 2002). As measured by the ratios of peak motion shown in Figure 5, the site amplification exists for all three measures of ground motion, but the amplification is clearly more sensitive to site class for peak acceleration than for peak displacement. There are consistent differences in the mean amplifications within each site class, with larger amplifications for sites underlain by lower-velocity materials. Much scatter, however, remains for the amplifications within each class, particularly for peak acceleration. The large

Figure 3. *Continued.*

station-to-station variability of ground motions within a given site class is a common finding in many studies.

NEHRP classes are also an effective way of grouping the amplifications given both by response spectra (Fig. 6) and by Fourier spectra (Fig. 7), and more information about the periods corresponding to the site amplifications are given by such amplifications than in amplifications corresponding to peak ground acceleration, velocity, and displacement. As with the ratios of peak motions, the amplifications shown in Figures 6 and 7 are clearly separated by site class. At frequencies less than about 2 Hz the amplification is largest for site class D, and the deamplification at higher frequencies is also largest for site class D. This is qualitatively expected as the result of the trade-off between increased amplification and increased attenuation for the lower-velocity materials characterizing class D sites. Of particular interest are the large site amplifications at periods much longer than used in previous studies of site amplification in Anchorage (the range of the previous studies is shown by the double-sided arrows in Figures 6 and 7); these amplifications persist to

periods of about 14 sec and are observable because of the relatively large radiation at long periods for the Denali fault earthquake. Comparisons are given in Figure 6 of the observed amplification with those in the 2000 NEHRP building code. Although the increase or decrease relative to unity is the same for the observed and the NEHRP amplifications, the values of the amplifications are in poor agreement with the longer-period motions at both class D and class B sites, being underpredicted by the NEHRP code relative to motions on class C sites (class D relative to class C at short periods being an exception).

Although engineers often characterize site response as ratios of response spectra, caution is needed in the interpretation of response spectral amplifications, particularly at short oscillator periods where the actual ground motion may be devoid of energy. Because the short-period asymptote of a response spectrum is controlled by the peak ground acceleration, the ratios of response spectra at short periods will equal the ratios of the peak accelerations, and the apparent amplification may not represent true high-frequency ground-
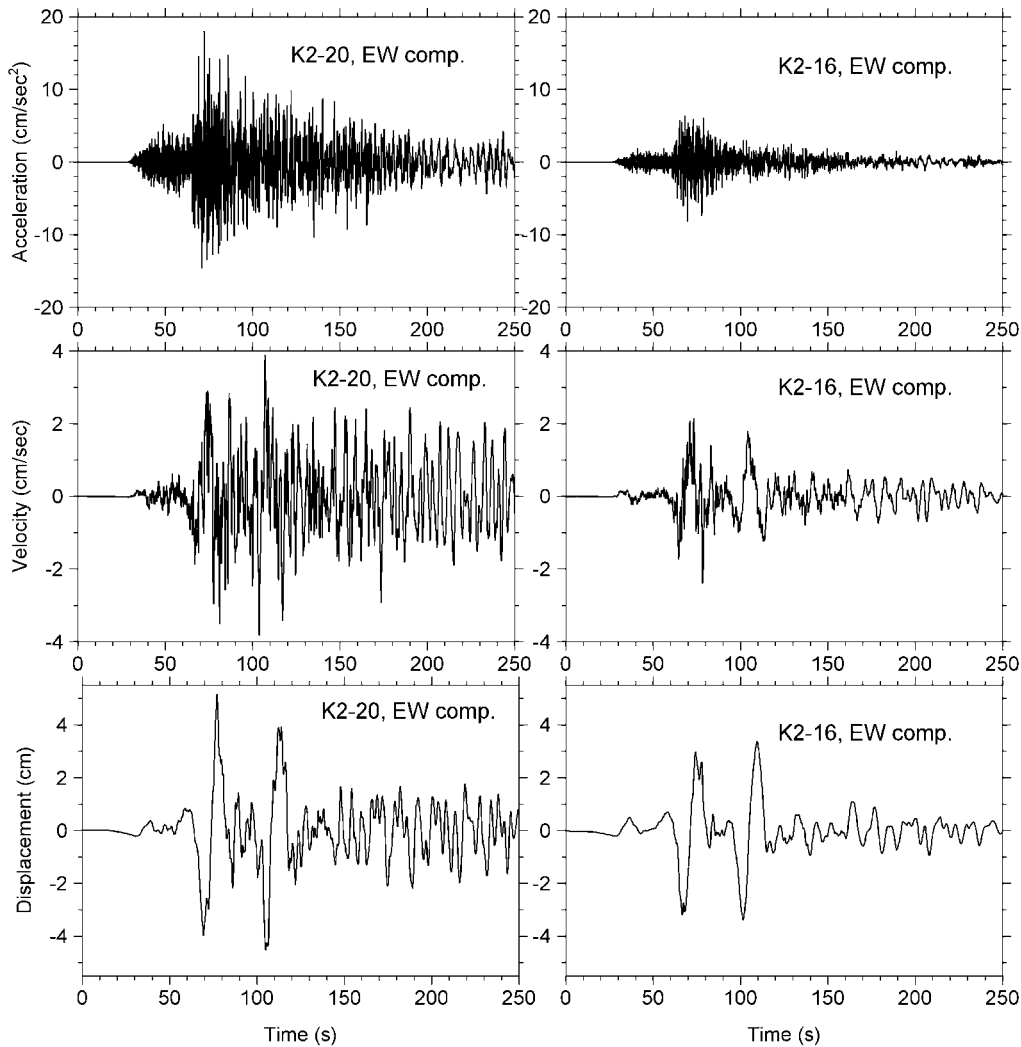
Figure 4.   Accelerations, velocities, and displacements at stations K2-20 and K2-16 for the east–west component.

motion amplification if the peak accelerations are controlled by frequencies less than the oscillator frequencies. In the present results this is clearly seen by comparing the response spectral and Fourier spectral amplifications at frequencies above about 8 Hz (Figs. 6, 7). The class C/D and class D response spectra show an apparent amplification at higher frequencies, consistent with the peak acceleration ratios shown in Figure 5. But they should not be interpreted as indicating greater site amplification at high frequencies for lower-velocity sites. In fact, as Figure 7 shows, the opposite is true: there is a deamplification at frequencies greater than 8 Hz for class D sites.

Spatial Variation

The previous figures showing site amplifications have largely dealt with amplifications within site classes. But what of spatial variation? Given the relatively large number of stations in the Anchorage area, and the nonrandom distri-

bution of site classes, it is possible to construct a map of site amplifications. This has been done for amplifications of motions at four frequencies, ranging from 0.2 to 14 Hz; the results are shown in Figure 8. Although some of the variation is clearly controlled by a single station, these maps show systematic trends not captured by simply looking at amplifications in a site class. In particular, note the increase of amplification toward the west for low-frequency motions. The trend for the 0.2 Hz motions roughly corresponds to increasing depth to bedrock. The spatial variations at higher frequencies may be due to local variations in near-surface geology, as discussed in some detail by Dutta *et al.* (2001), Martirosyan *et al.* (2002, 2004), Nath *et al.* (2002), and Dutta *et al.* (2003).

Comparison with Previous Studies

For periods common both to previous studies and to this study I made quantitative comparisons of the site amplifi-
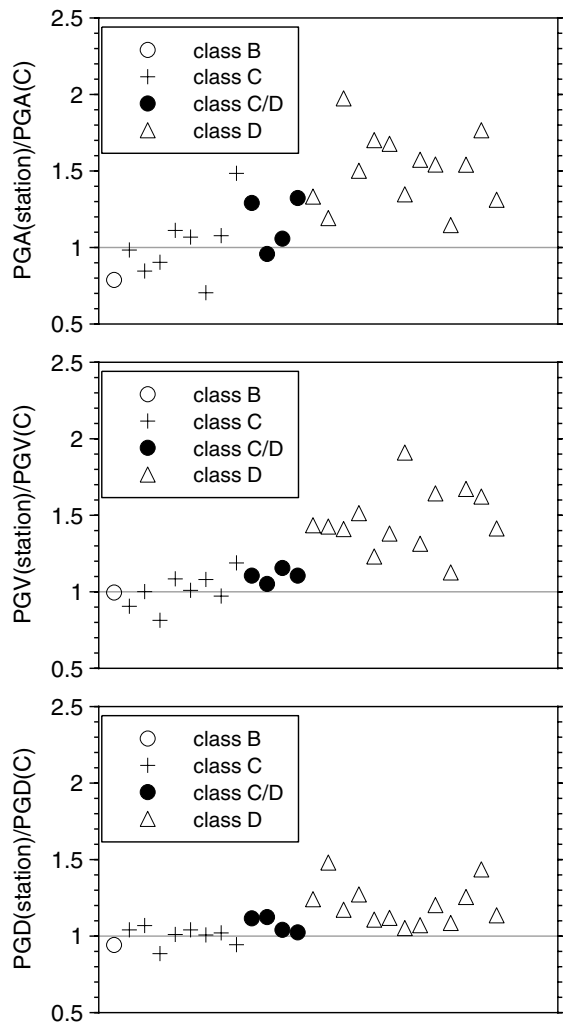
Figure 5.   Peak accelerations, velocities, and displacements, relative to the geometric mean of motions on class C sites, grouped by site class. All motions are oriented east–west.

cations. Figure 9 shows a comparison of site amplification from Martirosyan *et al.* (2002) at two stations, relative to K2-16. The amplification has been computed both from Fourier spectra and response spectra. Focusing only on the Fourier spectra amplification, the comparison is relatively good for station K2-01 in that the frequencies of amplification peaks coincide, as does the general level of amplification. The comparison for K2-02 is not as good, particularly above 2 Hz. Figure 10 shows another comparison, in this case of averages of Fourier spectra over two frequency bands. The amplifications are more compatible for the lower-frequency band (0.5–2.5 Hz) than for the higher-frequency band (3.0–7.0 Hz), although there is much scatter within each band. It is not surprising to see this scatter, as many studies find significant event-to-event variation for a single station pair and station-to-station variation for a single event (see, e.g., the review by Boore, 2004).

Displacement Pulses

Comparison with Pulses from 1999 Hector Mine, California, Earthquake

One of the interesting features of the recordings in Anchorage is the displacement pulses. This section discusses a few things associated with these pulses: the differing frequency content of the pulses, the similarity to pulses from a smaller earthquake occurring in California, and the contribution of the pulses to the long-period response spectral shape.

As noted before, the maximum accelerations are associated with pulse 2. The consequence of this is clearly seen by comparing response spectra for the whole record with those computed for the portions of the records corresponding to the two largest displacement pulses (pulses 2 and 3). The results are shown in Figure 11 for stations K2-20 and K2-16. Nearly all of the response at periods shorter than 1 sec and 4 sec is contributed by pulse 2 for stations K2-20 and K2-16, respectively, but both pulses contribute essentially equally to the peak in the spectra between 10 and 20 sec. The richness of high-frequency radiation of subevent 1 (corresponding to pulse 2) relative to subevents 2 and 3 was noted by Frankel (2004); my results illustrate the same conclusion using a different measure of ground motion.

I was struck with the similarity of the displacement pulses in Anchorage from the **M** 7.9 Denali fault earthquake with the pulse radiated by the **M** 7.1 1999 Hector Mine, California, earthquake (see Boore *et al.*, 2002). To make a quantitative comparison of the pulses, two copies of a representative pulse from the Hector Mine earthquake are superposed on the K2-03 record of the Denali fault earthquake in Figure 12. The Hector Mine motion is the transverse displacement from a station at an azimuth approximately normal to the strike-slip faulting in the Hector Mine earthquake (see Fig. 1 by Boore *et al.*, 2002); the displacement pulse was shifted to match the arrival times of the Denali earthquake pulses, and its amplitude was multiplied by 0.38 to correct for differences in propagation distances. The factor of 0.38 was obtained by evaluating the ground-motion prediction equations of Sadigh *et al.* (1997) for magnitude 7.1 and for the closest source-to-station distances for the 1999 and 2002 earthquakes. The Sadigh *et al.* (1997) equations were chosen because they were used by Wesson *et al.* (1999) in constructing probabilistic hazard maps for Alaska. The acceleration times series leading to the displacements were processed in identical ways for both earthquakes (note that the results of Boore *et al.*, 2002, used a causal low-cut filter rather than the acausal low-cut filter used here; the displacement waveforms can be quite different for the two types of filters). The waveforms and amplitudes for the two events are similar, consistent with the finding of Frankel (2004) that pulses 2 and 3 correspond to subevents of moment magnitude similar to that of the 1999 earthquake (7.1 and 7.0, compared to 7.1 for the Hector Mine earthquake). Although
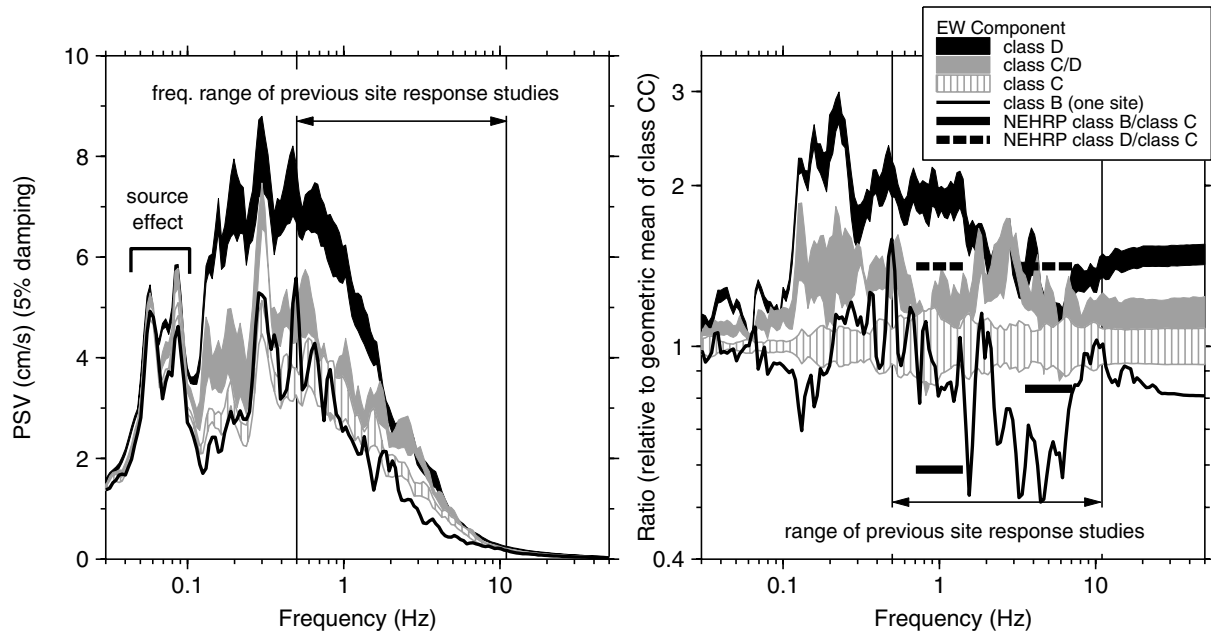
Figure 6. Range of standard error of the geometric means of 5%-damped pseudo relative velocity (PSV) response spectra of the east–west motion for recordings on the same NEHRP site class, and ratio of the range of standard error of the geometric means relative to the geometric mean of the spectra on class C sites. The short, wide bars are the site amplifications from the 2000 NEHRP building code (BSSC, 2001). For purposes of comparing with a subsequent plot of Fourier amplitude spectra, frequency rather than period is used for the abscissa.

Figure 7. Range of standard error of the geometric means of smoothed Fourier amplitude spectra of the east–west component accelerations recorded on the same NEHRP site class, and ratio of the range of standard error of the geometric means relative to the geometric mean of the spectra on class C sites. The individual spectra were smoothed with a triangular smoothing operator with a base width of 1 Hz.
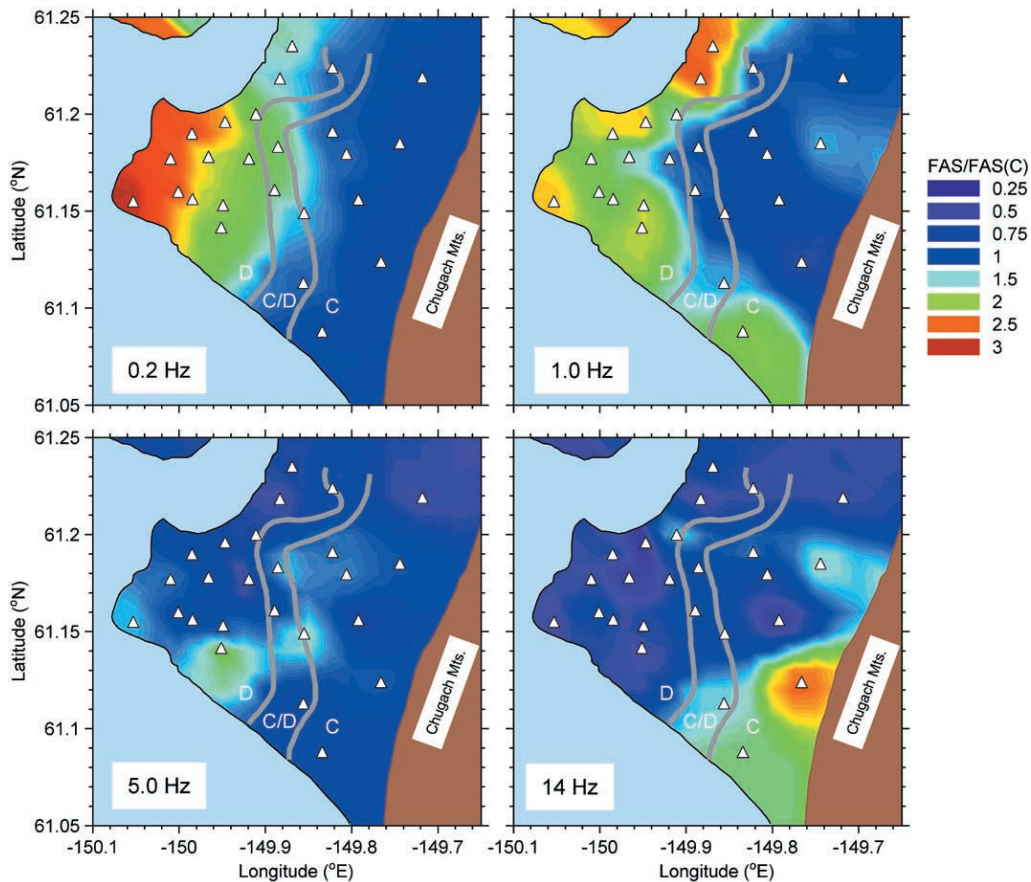
Figure 8.   Maps of site amplifications in the sediments to the west of the Chugach Mountains, relative to the geometric mean of motions on class C sites (the brown area shows the location of the Chugach Mountains; it is not site response). The amplifications were smoothed over short frequency intervals surrounding the center frequencies of 0.2, 1.0, 5.0, and 14.0 Hz. The stations used in constructing the map are shown by triangles; they are included to help in judging if amplification patterns are controlled by a single station (as is the case for the high amplifications near the Chugach Mountains for 14 Hz).

the displacement pulses are similar, close inspection shows that the pulses from the Denali fault earthquake have a somewhat longer duration. This leads to relatively more long-period content in the response spectra for the Denali fault motions (Fig. 13), although for both earthquakes the displacement response spectra are peaked for periods longer than 10 sec. It is important to note that the peaks are most likely due to the source and not to local site response. Are the large, long-period motions affected by source directivity (e.g., Somerville *et al.*, 1997)? Probably not, at least for the Hector Mine recording and pulses 2 and 3 for the Anchorage recordings from the Denali fault earthquake. In these cases the angle between the direction of fault rupture and the direction from the fault to the station is close to 90°, a directivity-neutral direction (the angle from the rupture direction to station K2-16 is 96° and 121° from subevents 2 and 3, respectively). The azimuth to Anchorage from subevent 1 is 66° from the strike of the subevent, but Frankel (2004) modeled the subevent as a point source, with no rup-

ture propagation. For this reason I cannot assess the relative importance of directivity for displacement pulse 2.

Pulses, Displacement Spectra, and Code Spectra

The relatively broad peaks in the displacement response spectra from about 8 to 15 sec is a feature not included in most spectra used for engineering design (e.g., Bommer and Elnashai, 1999). Many code spectra assume an increase without limit at long periods, whereas others impose a constant level for periods longer than about 2 to 4 sec. As shown by the comparisons in Figure 14, neither assumption is in agreement with the spectra in Anchorage from the Denali fault earthquake (and with reference to Fig. 13, the Hector Mine earthquake). Of course the observation of enhanced source-related long-period peaks in response spectra from only two earthquakes is not enough to produce a change in schemes for constructing engineering design spectra. Recent studies of data from the increasing number of modern broad-
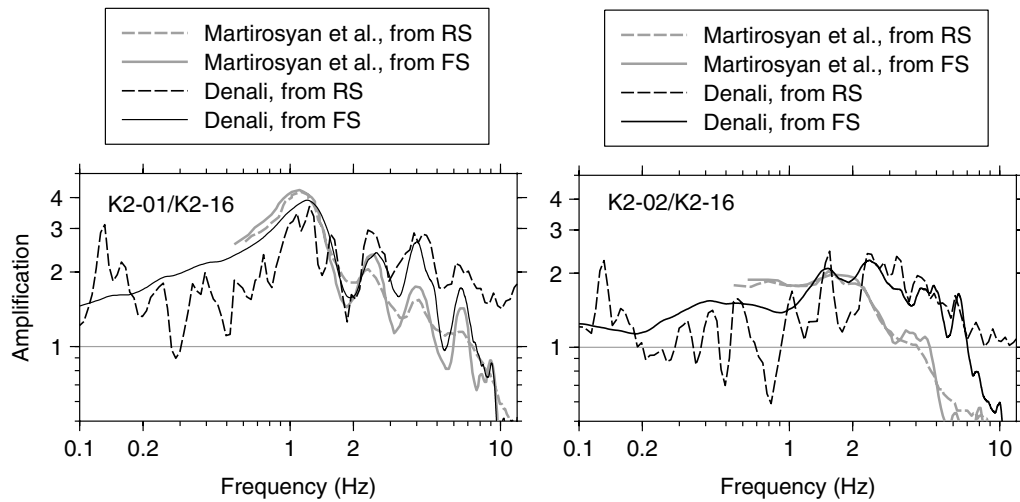
Figure 9. Site response at nearby stations K2-01 and K2-02, relative to K2-16, computed from Fourier amplitude spectra (FS) and response spectrum (RS). (K2-01 is site class D, whereas K2-02 is site class C/D). Shown are the site responses from the Denali fault earthquake ground motion and from the averages of 46 events, as determined by Martirosyan *et al.* (2002) (rms of the two horizontal components). The east–west component of motion was used for the Denali fault earthquake recordings. The Fourier spectra were smoothed before computing the ratios.
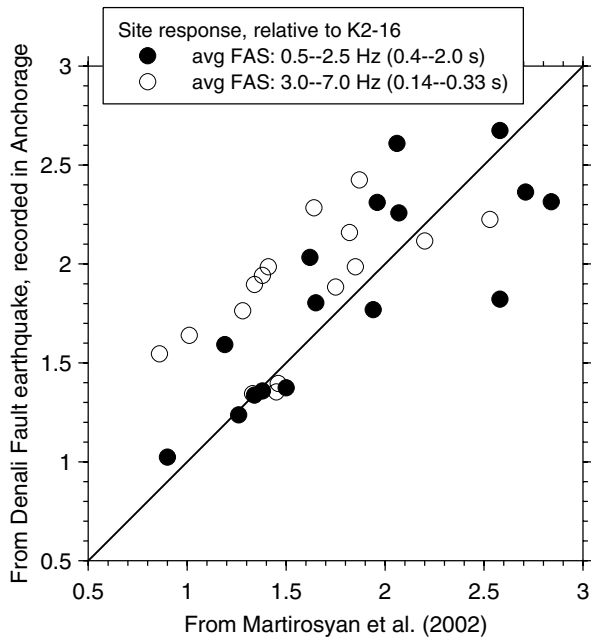

Figure 10. Comparison of site responses (relative to station K2-16) from smoothed Fourier amplitude spectra (FAS), as determined from the Denali fault earthquake data (east–west component) and from Martirosyan *et al.* (2002) (rms of the two horizontal components).

band digital recorders, as well as simulations of ground motion, have led to the introduction of a transition period in the 2003 NEHRP code that determines where the design spectral displacement becomes flat. This transition period is a mapped quantity and varies spatially in a way that roughly depends on the magnitude of the dominant earthquake for a given location determined from disaggregation of a probabilistic seismic hazard map. The transition period is 16 sec for recordings in Anchorage and 8 sec for the Hector Mine recording. Using the new code to construct the design motions for Anchorage results in a spectrum remarkably similar to the observed spectrum (Fig. 14), and the agreement with the Hector Mine spectrum, although not shown, would be equally good (the Anchorage recordings of the Denali fault earthquake were not used in constructing the transition-period maps (C. B. Crouse, personal comm., 2004)).

Summary

This purely observational study of digital strong-motion data from the 2002 Denali fault earthquake recorded in and near Anchorage, Alaska, finds a number of systematic features in the ground motion. In agreement with previous studies, the data show significant ground-motion amplification. The amplifications are well differentiated by NEHRP site class, with the class D amplification exceeding a factor of 2 relative to an average of motions on class C sites. New to this study is the finding that the site amplification extends to periods of at least 10 sec.
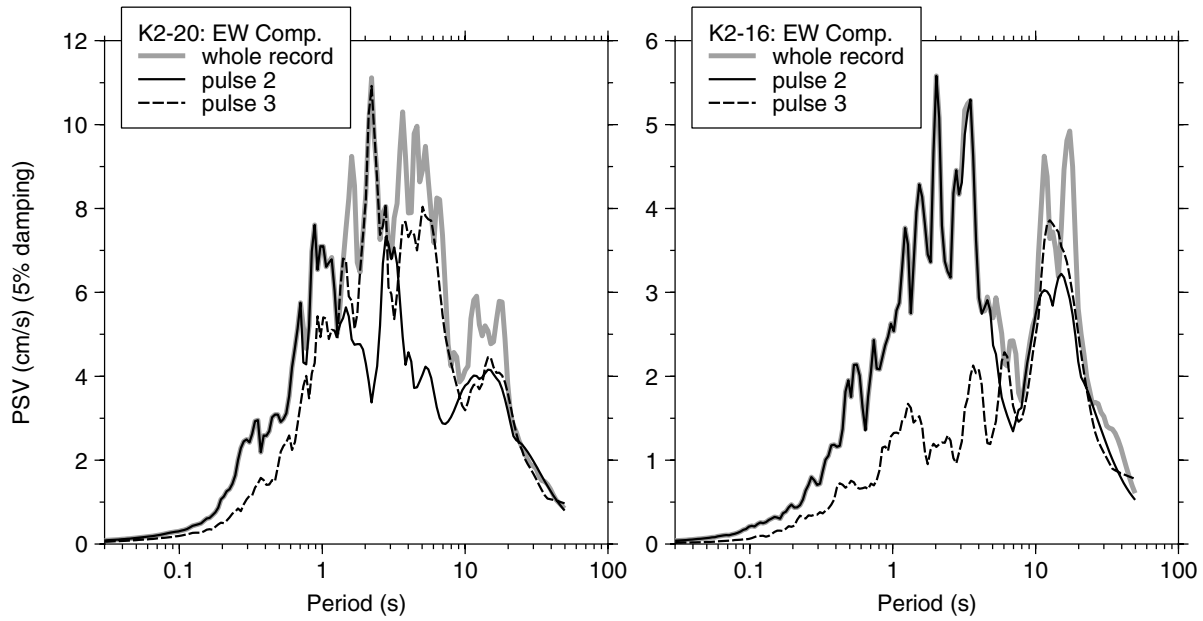
Figure 11.   5%-damped pseudo relative velocity (PSV) response spectrum for the east–west component at stations K2-20 and K2-16, from the whole record and from windows that include separately the two large displacement pulses (pulses 2 and 3 in Fig. 2). The portions of the accelerograms have different influences on the response spectra. From the acceleration trace (Fig. 4), it is clear that most of the energy at high frequencies is carried in pulse 2, so the response spectra from that pulse is essentially equal to the whole record response spectrum at shorter periods. Conversely, for this record pulses 2 and 3 contribute about equally to the longer-period response.
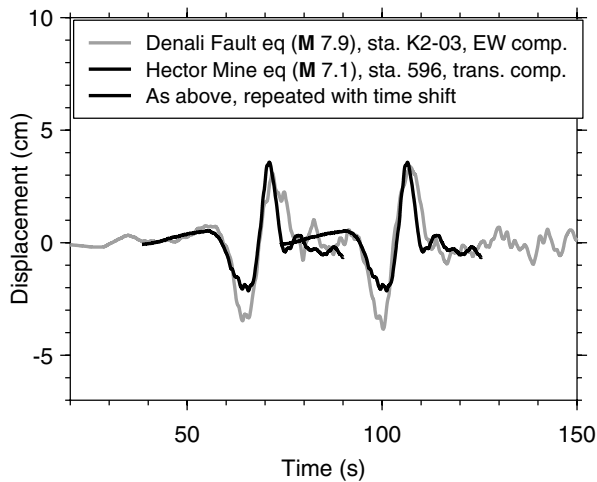

Figure 12.   East–West displacements from station K2-03 from the Denali fault earthquake. Superimposed are two copies, shifted in time, of the transverse displacements from the instrument 596 recording of the Hector Mine (HM) earthquake. The HM motions have been divided by 2.6 to correct for the different distances to the earthquakes. The factor of 2.6 came from the ground-motion prediction equations of Sadigh *et al.* (1997). All records were low-cut filtered with a low-order acausal butterworth filter with a corner at 0.02 Hz (the filter response goes as f^4 for low frequencies).
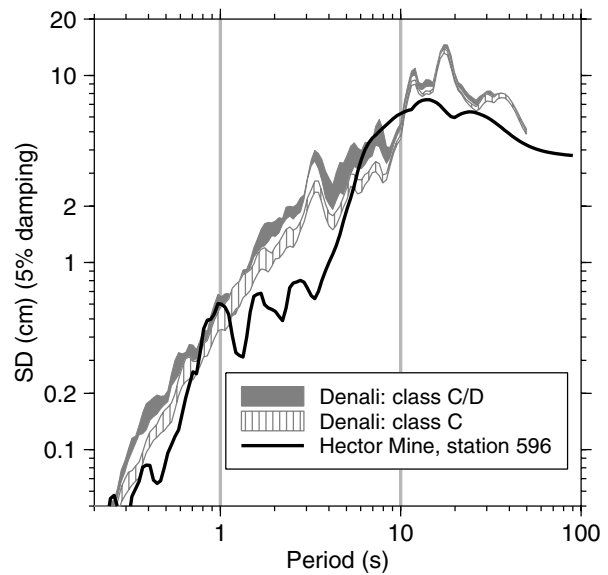

Figure 13.   Displacement response spectrum (SD) for the Denali fault earthquake recordings and for the transverse component of the 1999 Hector Mine, California, earthquake (after dividing the Hector Mine spectrum by 2.6 to correct for the different distances to the earthquakes). All records were low-cut filtered with a low-order acausal butterworth filter with a corner at 0.02 Hz (the filter response goes as f^4 for low frequencies).
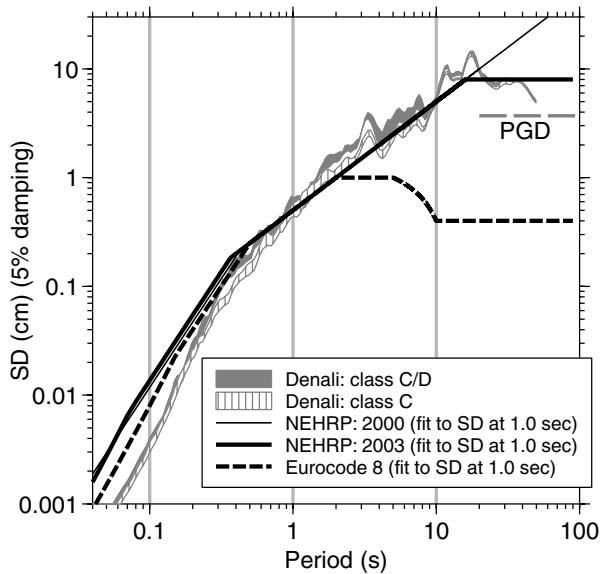
Figure 14. Comparison of observed displacement response spectrum (SD) for class C/D and C sites in Anchorage to the spectra constructed following the procedures for the following building codes: 2000 NEHRP (BSSC, 2001), 2003 NEHRP (BSSC, 2004), and Eurocode 8 (CEN, 1998). Also shown is the peak ground displacement (PGD) for the Anchorage motions; the displacement response spectrum will by asymptotic to this value at suffciently long periods. For NEHRP, the mapped values of spectral response at 0.2 and 1.0 sec were used, but to emphasize the shape, the spectra for the three codes have been normalized to a representative value of the data at 1.0 sec.

The long-period ground displacements are characterized by a series of distinct pulses, corresponding to the subevents along the fault identified in source inversion studies (e.g., Frankel, 2004). The two largest pulses are similar in shape and amplitude to the pulse radiated by the 1999 Hector Mine, California, earthquake. The moment magnitude of that earthquake (7.1) is similar to the moment magnitudes inferred for subevents 1 and 2 of the Denali fault earthquake (7.1 and 7.0, respectively [Frankel, 2004]). These pulses produce a localized long-period peak in response spectra, with the peak for the Denali recordings being at a somewhat longer period than for the Hector Mine earthquake recordings. The pulses have polarizations that are similar for all stations and show a systematic clockwise rotation from pulse 2 to pulse 4, consistent with *SH* waves radiated from localized sources along the fault progressively to the east of the hypocenter. As noted by Frankel (2004), most of the high-frequency motion is carried by the *S*-wave pulse from subevent 1; the other subevents apparently radiated relatively little high-frequency energy. The design spectra from the well-known 2000 NEHRP and the Eurocode 8 building codes disagree with the displacement response spectrum from both the Hector Mine and the Denali fault earthquakes in completely different ways: the 2000 NEHRP displacement spectrum increases

without limit, whereas the Eurocode 8 displacement spectrum is constant or decreases for periods longer than 2 sec; the observed spectra for the two earthquakes studied here flatten at periods slightly in excess of 10 sec. The Denali fault spectrum is, however, in good agreement with the recently adopted 2003 NEHRP building code.

Acknowledgments

References

Bommer, J. J., and A. S. Elnashai (1999). Displacement spectra for seismic design, *J. Earthquake Eng.* **3,** 1–32.

Boore, D. M. (1999). Basin waves on a seafloor recording of the 1990 Upland, California, earthquake: implications for ground motions from a larger earthquake, *Bull. Seism. Soc. Am.* **89,** 317–324.

Boore, D. M. (2004). Can site response be predicted? *J. Earthquake Eng.* **8,** Special Issue 1, 1–41.

Boore, D. M., C. D. Stephens, and W. B. Joyner (2002). Comments on baseline correction of digital strong-motion data: examples from the 1999 Hector Mine, California, earthquake, *Bull. Seism. Soc. Am.* **92,** 1543–1560.

Building Seismic Safety Council (BSSC) (2001). *NEHRP Recommended Provisions for Seismic Regulations for New Buildings and Other Structures, 2000 Edition, Part 1: Provisions*, report prepared by the Building Seismic Safety Council for the Federal Emergency Management Agency (Report No. FEMA 368), Washington, D.C. Available from www.bssconline.org/NEHRP2000/comments/provisions/ (last accessed December 2004).

Building Seismic Safety Council (BSSC) (2004). *NEHRP Recommended Provisions for Seismic Regulations for New Buildings and other Structures, 2003 Edition, Part 1: Provisions; Part 2: Commentary*, report prepared by the Building Seismic Safety Council for the Federal Emergency Management Agency (Report No. FEMA 450), Washington, D.C. Available from www.bssconline.org/ (last accessed December 2004).

Dutta, U., N. Biswas, A. Martirosyan, S. Nath, M. Dravinski, A. Papageorgiou, and R. Combellick (2000). Delineation of spatial variation of shear-wave velocity with high frequency Rayleigh wave, *Geophys. J. Int.* **143,** 365–376.

Dutta, U., N. Biswas, A. Martirosyan, A. Papageorgiou, and S. Kinoshita (2003). Estimation of earthquake source parameters and site response in Anchorage, Alaska, from strong-motion network data using generalized inversion method, *Phys. Earth Planet. Interiors* **137,** 13–29.

Dutta, U., A. Martirosyan, N. Biswas, A. Papageorgiou, and R. Combellick (2001). Estimation of *S*-wave site response in Anchorage, Alaska, from weak-motion data using generalized inversion method, *Bull. Seism. Soc. Am.* **91,** 335–346.

Eberhart-Phillips, D., P. J. Haeussler, J. T. Haeussler, J. T. Freymueller, A. D. Frankel, C. M. Rubin, P. Craw, N. A. Ratchkovski, G. Anderson, G. A. Carver, A. J. Crone, T. E. Dawson, H. Fletcher, R. Hansen, E. L. Harp, R. A. Harris, D. P. Hill, S. Hreinsdóttir, R. W. Jibson, L. M. Jones, R. Kayen, D. K. Keefer, C. F. Larsen, S. C. Moran, S. F. Personius, G. Plafker, B. Sherrod, K. Sieh, N. Sitar, and W. K. Wallace (2003). The 2002 Denali fault earthquake, Alaska: a large magnitude, slip-partitioned event, *Science* **300,** 1113–1118.

European Committee for Standardization (CEN) (2002). Eurocode 8: Design of structures for earthquake resistance, Draft No. 5, CEN Doc CEN/TC250/SC8/N317 (prEN 1998-1:200X), Brussels.

Frankel, A. (2004). Rupture process of the **M** 7.9 Denali fault, Alaska, earthquake: Subevents, directivity, and scaling of high-frequency ground motions, *Bull. Seism. Soc. Am.* **94,** no. 6B, S234–S255.

Hartman, D. C., G. H. Pessel, and D. L. McGee (1974). Stratigraphy of the Kenai group, Cook Inlet, *Alaska Div. Geol. Geophys. Surv. Open-File Rept. 49*. Available at www.dggs.dnr.state.ak.us/pubs/pubs?reqtype =citation&ID=149 (last accessed December 2004).

Martirosyan, A., and N. Biswas (2002). Site response at a rock site in Anchorage, Alaska from borehole strong-motion records (abstract), *Seism. Res. Lett.* **73,** 267.

Martirosyan, A., N. Biswas, U. Dutta, D. Cole, and A. Papageorgiou (2004). Ground motion analysis in the Anchorage basin: 1-D approach, *J. Earthquake Eng.* **7,** 251–274.

Martirosyan, A., U. Dutta, N. Biswas, A. Papageorgiou, and R. Combellick (2002). Determination of site response in Anchorage, Alaska, on the basis of spectral ratio methods, *Earthquake Spectra* **18,** 85–104.

Nath, S. K., D. Chatterjee, N. N. Biswas, M. Dravinski, D. A. Cole, A. Papageorgiou, J. A. Rodriguez, and C. J. Poran (1997). Correlation study of shear-wave velocity in near-surface geological formations in Anchorage, Alaska, *Earthquake Spectra* **13,** 55–75.

Nath, S. K., N. N. Biswas, M. Dravinski, and A. S. Papageorgiou (2002). Determination of *S*-wave site response in Anchorage, Alaska, in the 1–9 Hz frequency band, *Pure Appl. Geophys.* **159,** 2673–2698.

Sadigh, K., C.-Y. Chang, J. A. Egan, F. Makdisi, and R. R. Youngs (1997). Attenuation relationships for shallow crustal earthquakes based on California strong motion data, *Seism. Res. Lett.* **68,** 180–189.

Somerville, P. G., N. F. Smith, R. W. Graves, and N. A. Abrahamson (1997). Modification of empirical strong ground motion attenuation relations to include the amplitude and duration effects of rupture directivity, *Seism. Res. Lett.* **68,** 199–222.

Wesson, R. L., A. D. Frankel, C. S. Mueller, and S. C. Harmsen (1999). Probabilistic seismic hazard maps of Alaska, *U.S. Geol. Surv. Open-File Rept. 99-36*, 20 pp.

U.S. Geological Survey, MS 977
345 Middlefield Road
Menlo Park, California 94025
boore@usgs.gov